American Mineralogist, Volume 87, pages 947–957, 2002

Synthesis and NMR characterization (^{1}H and ^{31}P MAS) of the fluorine-free hydroxylapatite–britholite-(Y) series

JULIETTE IMBACH,[1] FABRICE BRUNET,[2,*] THIBAULT CHARPENTIER,[1] AND JOSEPH VIRLET[1]

[1]Service de Chimie Moléculaire, CEA Saclay, F-91191 Gif sur Yvette, France
[2]Laboratoire de Géologie, UMR 8538 CNRS, Ecole normale supérieure, 24 rue Lhomond, F-75005 Paris, France

ABSTRACT

Apatites in a fluorine-free chemical system have been synthesized hydrothermally at 650 °C and 1.5 kbar along the hydroxylapatite–britholite-(Y) join [i.e., $Ca_{10}(PO_4)_6(OH)_2$ – $Ca_4Y_6(SiO_4)_6(OH)_2$ join], from oxide mixtures at nominal Si-contents of 0, 0.5, 1, 2, 3, 4, 5.5, and 6 pfu. The hexagonal apatite unit-cell volume decreases by 1.5% from the phosphate to the silicate end-member. A single ^{31}P MAS NMR resonance is recognized at 2.8 ppm in hydroxylapatite. An additional broad line centered around 1.5 ppm is present for Y-rich compositions. Although the ^{31}P MAS NMR spectra could not be fully assigned, the 2.8 ppm resonance that persists even in Si-rich compositions must include the contribution of P atoms involved in P-O-Y bonds. ^{1}H NMR spectroscopy shows that the H content decreases by around 50% from the phosphate to the silicate end-member although all the compounds were synthesized hydrothermally at 650 °C. In addition to the expected $YSiCa_{-1}P_{-1}$ substitution, a second substitution vector, $Y\square Ca_{-1}H_{-1}$, is inferred. It is proposed that the resulting proton vacancies influence neighbor H atoms to give rise to a ^{1}H line at 4.9 ppm. Beside the 4.9 ppm resonance, four other resonances at 0.2, 1.2, 1.5, and 2.0 ppm, are encountered along the series. In the apatite columns, OH groups are bonded to three cations from the Ca2 site and form $(Ca2)_3OH$ groups. In the proposed assignment model, the 0.2 ppm line, the only resonance present in the hydroxylapatite spectrum, is readily attributed to protons from $(Ca)_3OH$ groups. The 1.2 and 1.5 ppm resonances are assigned to $(Ca_2Y)OH$ groups whereas the 2.0 ppm line represents the contribution of protons from both $(CaY_2)OH$ and $(Y)_3OH$ groups.

INTRODUCTION

Apatite, $Ca_5(PO_4)_3(F,OH,Cl)$, is the most widespread phosphate mineral in crustal rocks (McConnell 1973). In addition to be stable over a wide range of pressure and temperature conditions (Murayama et al. 1986; Brunet et al. 1999), the apatite structure is also remarkable for its wide chemical variability. The compositions of apatite group compounds can be expressed as $A_5(XO_4)_3(F,Cl,OH)$ with A = Ba, Ca, Ce, K, Na, Pb, Sr, Y; X = As, C, P, Si, S, V (Fleischer and Altschuler 1986). The chemical variability of the apatite structure becomes apparent when the wide spectrum of synthetic apatite compositions is considered (e.g., Ito 1968; Engel and Klee 1972; Boyer et al. 1997). Infrared spectroscopy has been successfully applied to identify specific structural features in apatite such as the occurrence of PO_3OH groups in Ca-deficient apatites or the presence of CO_3 or SiO_4 groups (Elliott 1964). For hydroxyl-bearing apatites, many Raman or IR spectroscopy studies have been carried out to decipher the halogen distribution in the apatite channels (e.g., Freund and Knobel 1976). In many cases, the interpretation of OH-vibration spectra is hampered by a poor understanding of hydrogen bonding in apatite. NMR spectroscopy studies of apatites are scarce and deal with phosphate apatites (Rothwell et al. 1980; Yesinowski and Eckert 1987; Belton et al. 1988). In the present study, we have combined ^{1}H and ^{31}P MAS as well as ^{1}H-^{31}P Cross Polarization NMR spectroscopy (CPMAS) along with FT-IR spectroscopy to investigate local atomic environments in apatite along the hydroxylapatite–britholite-(Y) join [i.e., the $Ca_{10}(PO_4)_6(OH)_2$ – $Ca_4Y_6(SiO_4)_6(OH)_2$ join]. The $Ca^{2+} + P^{5+} = REE^{3+} + Si^{4+}$ substitution ($REESiCa_{-1}P_{-1}$ with REE = Rare Earth Elements) occurs in natural apatites but very little is known about its crystal chemistry. This type of substitution is of interest because (1) Si-bearing apatites have been proposed as a possible repository for trivalent actinides from nuclear wastes, and (2) a second, naturally occurring, phosphate-to-silicate complete solid solution series has recently been discovered (Chopin and Sobolev 1995) that adopts the ellenbergerite structure.

Pure britholite-(Y) was chosen for this NMR study because, contrary to most REE elements, yttrium is not paramagnetic. Hydrothermal syntheses were adopted because they generally lead to homogeneous and well-crystallized products. This method was successfully applied by Ito (1968) to the synthesis of a wide variety of apatite-britholite members. Hydrothermal synthesis implies incorporation of OH-groups in the apatite product; therefore, to begin with, apatites in the CaO-P_2O_5-SiO_2-Y_2O_3-H_2O fluorine-free system were investigated.

Britholites are silicate-dominant REE-bearing members of the apatite group. Britholite is a major REE-bearing mineral (Mariano 1989) and is either Ce-dominant, britholite-(Ce), or

* E-mail: brunet@geologie.ens.fr

Y-dominant, britholite-(Y). These rare minerals are found in high-temperature geological settings such as high-grade contact metamorphic rocks (Jamtveit et al. 1997), carbonatites (Ouzegane et al. 1988), or volcanic ejecta (Della Ventura et al. 1999), where, in some instances, they can be related to late crystallization stages. The isomorphism between calcium-phosphate apatites and britholites proposed by Matchatshki (1939) has been unequivocally confirmed by single-crystal X-ray analyses of natural britholites (Kalsbeek et al. 1990; Noe et al. 1993). Although apatite-group minerals with various Si/P ratios are found in nature, complete solid solution between calcium-phosphate apatite and britholite has only been demonstrated experimentally. On the basis of hydrothermal experiments, Ito (1968) has shown that hydroxylapatite forms a complete solid-solution series with britholite-(Y) in the pure CaO-Y_2O_3-SiO_2-P_2O_5-H_2O system at 2 kbar. Other than some infrared spectroscopy measurements and water titrations, Ito (1968) mainly characterized his synthetic products using X-ray powder diffraction (XRPD). Khudolozhkin et al. (1973) also carried out a detailed XRPD study but on the pure-fluorine members of apatite-britholite series, to investigate partitioning of various rare-earth elements between the two apatite calcium sites.

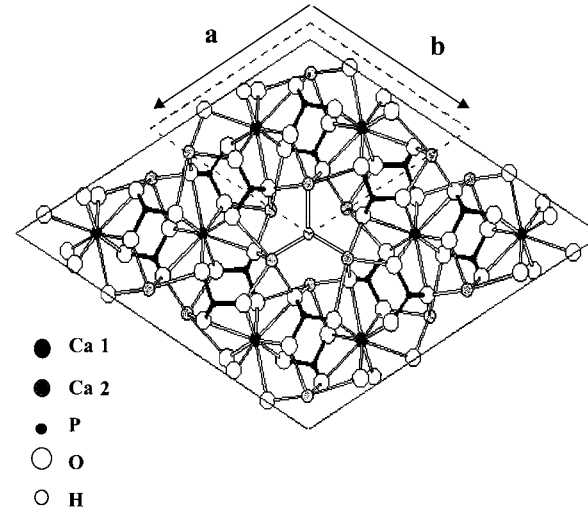

FIGURE 1. Projection of the hydroxylapatite structure onto the (**a**,**b**) plane. Dashed lines outline the unit cell. An apatite channel is seen at the center of the diagram. The hydroxyl O atom in the center of the channel is not represented to emphasize the H atom that would be otherwise hidden. Atomic coordinates are from Kay et al. (1964).

HYDROXYLAPATITE AND BRITHOLITE-(Y) ATOMIC ARRANGEMENT

Synthetic end-member hydroxylapatite is monoclinic $P2_1/b$ (Elliott et al. 1973) while fluorapatite, either synthetic or natural, crystallizes with a hexagonal unit cell ($P6_3/m$, Sudarsanan et al. 1972). F atoms, which occur in columns parallel to the **c** axis, are located on the mirror planes at $z = 1/4$ and 3/4 in fluorapatite, and in hydroxylapatite the OH groups sit 0.3 Å either above or below the mirror plane (Sudarsanan et al. 1972; Kay et al. 1964; Hughes et al. 1989). In synthetic end-member hydroxylapatite, the OH groups are all ordered above the mirror plane in a single column and below the plane in the adjacent column along **b** (Elliott et al. 1973; Hughes et al. 1989). This gives rise to a $P2_1/b$ monoclinic superstructure (Elliott et al. 1973). Surprisingly, natural hydroxylapatites crystallize with the hexagonal $P6_3/m$ symmetry (e.g., Kay et al. 1964; Hughes et al. 1989). Compared to the $P2_1/b$ symmetry, the addition of a mirror plane will generate two equivalent half-occupied positions with disordered OH anions in the columns. Because, in a column, two adjacent OH groups cannot point toward each other (short-range order constraint), clusters of OH groups pointing in the same direction must alternate in the columns to preserve long range disorder. To explain the hexagonal symmetry of natural hydroxylapatite, it has been proposed that OH vacancies or F atoms occur at points where the direction of the OH groups is reversed (Kay et al. 1964; Elliott et al. 1973).

The hydroxylapatite structure (Fig. 1) is based on a close packing of O atoms (Moore 1984). There are two distinct calcium sites (Ca1 and Ca2). Calcium atoms of the Ca1 site are in ninefold coordination with six short and three long Ca-O bonds (mean Ca-O distance 2.557 Å; Kay et al. 1964). Calcium atoms of the Ca2 site form CaO_6OH polyhedra (mean Ca-O distance = 2.452 Å; Kay et al. 1964). They form, in the mirror planes, triangles that alternate along the [001] hexad (Fig. 2).

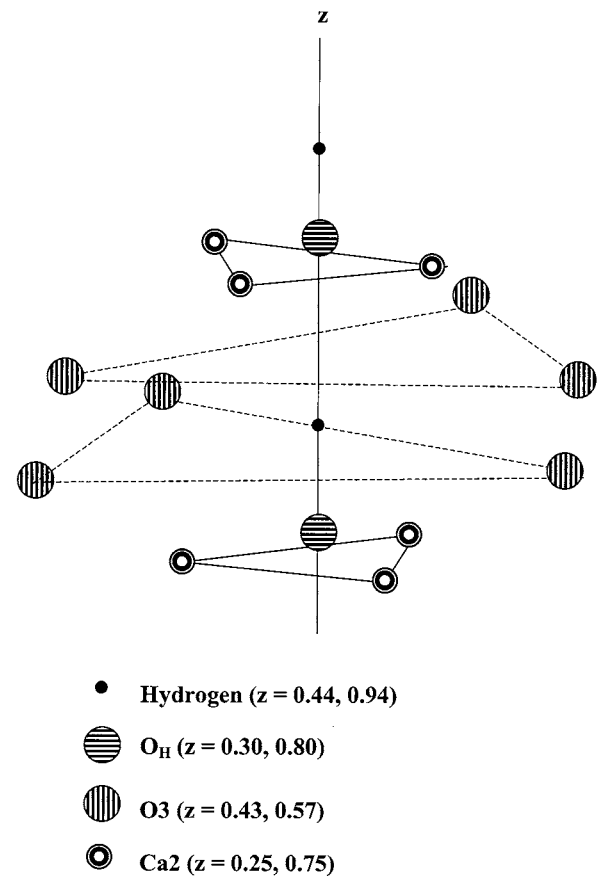

FIGURE 2. Local hydrogen atom environment in a hydroxylapatite channel. Ca2 atoms form a triangle in the mirror planes at $z = 1/4$ and 3/4. The H-O3 and H-O_H distances are 2.92 and 2.48 Å, respectively.

There is a single, tetrahedrally coordinated, phosphorus site (mean P-O distance = 1.536 Å; Kay et al. 1964). The phosphorus tetrahedron is connected to four Ca1 and five Ca2 polyhedra via edge or corner sharing.

The location of the H atoms in OH-apatite was determined by Kay et al. (1964) using neutron diffraction. Each hydrogen atom belongs to a $(Ca2)_3OH$ group. The three Ca2 atoms of that group form a triangle in the mirror plane (Fig. 2). The shortest Ca-H distance (2.69 Å) is found between atoms of the same group. The next three closest calcium atoms are from the next $(Ca2)_3OH$ group (Ca-H = 3.19 Å). Each hydrogen atom is surrounded by three O3 atoms at 2.92 Å. Apart from the donor O atom (O_H) – hydrogen distance of approximately 0.9 Å, the shortest O-H distance (2.48 Å) is realized with the O_H atom of the next $(Ca2)_3OH$ group. The occurrence of hydrogen bonding in hydroxylapatite has been a matter of debate (e.g., Baddiel and Berry 1966; Engel and Klee 1972; Gonzales-Diaz and Santos 1977). According to the H···O distances derived from neutron diffraction data, the best candidates as potential acceptor O atoms are the hydroxyl O atom (O_H) at 2.54 Å (e.g., Engel and Klee 1972; Baumer et al. 1994). For such large distances, however, hydrogen bonding can only be marginal (Libowitzky 1999).

The structure of natural fluorine-rich britholite-(Y) was solved by Noe et al. (1993). They confirmed the general apatite atomic arrangement but found that the space group was $P2_1$ instead of the hexagonal $P6_3$ group determined by Kalsbeek et al. (1990) for britholite-(Ce). Because of the monoclinic symmetry of britholite-(Y), additional degenerate sites must be considered. The symmetry difference between phosphate apatites and britholites is mainly due to the O3 arrangement around Ca1. In both types of apatite, the 1-site cation sits on the (*f*) special position. In phosphate apatites, each ninefold coordinated polyhedron displays three long Ca-O3 bonds. In hexagonal britholites ($P6_3$), some of the Ca-O3 bonds are short but a given CaO_9 polyhedron has either three short or three long Ca-O3 bonds and therefore only the mirror operation is lost. In monoclinic britholites, the 1-site is split into two sites designated REE1a and REE1b. The REE1a site displays one long and two short REE-O3 bonds, whereas REE1b has two long and one short REE-O3 bonds. The threefold operation is therefore lost and these britholites are monoclinic.

Synthesis procedure

Starting material was prepared by grinding in an agate mortar $CaCO_3$ (Merck, suprapur), decarbonated beforehand at 1000 °C for 2 hours, and $NH_4H_2PO_4$ (Aldrich, 99.999%) in stoichiometric proportion. The resulting powder was heated at 600 °C for 3 hours in a platinum crucible, and ground a second time along with Y_2O_3 (Strem Chemicals, 99.99%) and amorphous silica (Merck, 99.9%), if required. A gold capsule was filled with the stoichiometric mixture and deionized water (fluid-solid ratio around 7 wt%), and was welded shut. The sample was loaded in a Tuttle-type cold-seal vessel placed horizontally in an external furnace. All syntheses were performed at 1.5 kbar and 650 °C for a duration of one or two weeks. Water pressure was measured with a Bourdon gauge. Temperature was measured with an outer Ni-NiCr thermocouple and regulated within 1 °C. At the end of the run, the vessel was cooled under an air stream. In addition, YPO_4 and YOOH compounds were synthesized hydrothermally at 450 °C, 3.5 kbar (from a stoichiometric mixture of Y_2O_3 and $NH_4H_2PO_4$) and 650 °C, 1.5 kbar (from Y_2O_3), respectively. These synthetic materials were used as references to interpret some of the spectroscopic results. Additional heating experiments were performed at 1 bar in air on some of the hydrothermal apatite-products. The sample was loaded in a platinum crucible and was placed in a muffle furnace. The power to the furnace was switched off after the experiment so that the sample would cool slowly.

Characterization techniques

X-ray powder diffraction (XRPD)

X-ray powder diffraction was performed using a Philips diffractometer in θ-2θ geometry (Cu$K\alpha$ radiation). Sample powders were mounted on a glass slide. Lattice parameters were determined by Rietveld refinement (DBW-9006PC, Sakthivel and Young 1991) in the (5–100°) 2θ-range. Silicon powder (NBS standard) was used as internal standard to adjust both sample displacement and zero-point parameters. The unit-cell parameters were refined assuming a hexagonal cell. The atomic coordinates of Hughes et al. (1989) were used but not refined.

Infrared spectroscopy

Infrared spectra were recorded using a FT-IR Perkin-Elmer 1725X spectrometer in the 3750–2750 cm^{-1} region. Spectra were averaged over 50 scans with a nominal resolution of 2 cm^{-1}. Ten milligrams of sample powder were intimately mixed with 100 mg of KBr. The mixture was dried for one hour at 110 °C and was then pressed into a pellet. All spectra (background and sample) were recorded under an argon flow.

^{31}P and ^{1}H MAS NMR

Solid-state ^{1}H and ^{31}P MAS NMR as well as ^{1}H-^{31}P cross polarization spectra were acquired on a Bruker 300 (7.1 T) and 500 (11.7 T) AVANCE spectrometers with a 4 millimeter MAS probe operating at, respectively, (^{1}H) = 300.13 and 499.14 MHz, (^{31}P) = 121.49 and 202.05 MHz. ^{31}P NMR spectra were recorded using a single 90° pulse excitation at a spin rate ν_r = 12.5 kHz. The 90° pulse width was 1.25 µs and the recycle delay 300 s. For ^{1}H NMR the probe background signal was minimized by the use of an anti-ringing sequence composed of two acquisition steps. The first consists of one 180° pulse followed by a time delay (of around 20 ms, greater than T_2) and a 90° pulse. Because protons far from the coil are much less sensitive to pulse length than protons of the sample, the acquired signal corresponds to the probe background minus the sample signal. The second acquisition step consists of only one 90° pulse, and the signal obtained is the sum of the probe background and the sample signal. The subtraction of the signals obtained at each of these two steps leads to a signal cleared of artifacts. The 90° and 180° pulse widths were, respectively, 1.85 µs and 3.7 µs, and the recycle delay was 120 s. For both nuclei, 8 transients and 8 dummy-scans were used, to avoid non reproducible signal amplitudes. T_1 of around 300 seconds for ^{31}P and 20 sec-

onds for ^{1}H were measured for hydroxylapatite. Chemical shifts are reported relative to an external standard set to 0 ppm: tetramethylsilane (TMS) for ^{1}H and an aqueous solution of phosphoric acid (85% H_3PO_4) for ^{31}P.

To compare ^{1}H NMR signals obtained from various samples in a quantitative way, all spectra were recorded under identical operating conditions. Assuming that the synthetic apatite has the nominal stoichiometry of the starting powder mixture, the line intensities were normalized to an identical number of moles and calibrated to hydroxylapatite. The measured samples were also used for another study (dehydration experiments) so no internal standard material was added. Based on ^{1}H MAS NMR measurements on adamantane-SiO_2 mixtures of seven different molar ratios, the uncertainty on inferred proton contents is estimated to be around 5%.

Individual line parameters were modeled using the computer program WINFIT (Massiot et al. 1994). The shape of the well-resolved hydroxylapatite lines, either ^{31}P or ^{1}H, were best fitted using a "50% LORENTZIAN - 50% GAUSSIAN" shape. This lineshape was applied to all lines (^{31}P or ^{1}H). The intensity of each resonance was determined by multiplying its half-width by its height. For a spin rate of ν_r = 12.5 kHz, spinning sidebands have so weak an intensity that their contribution can be neglected.

Cross-polarized one-dimensional ^{1}H-^{31}P MAS NMR experiments (1D CP/MAS NMR) were performed at ν_r = 5 kHz using a 90° proton pulse of 1.85 μs and a mixing period τ of 2 ms. For polarization transfer from proton to phosphorus, the magnitude of the proton and phosphorus radiofrequency fields were matched to fulfill the Hartmann-Hahn condition (Hartmann and Hahn 1962):

$$\gamma_{^1H} H^1_{^1H} = \gamma_{^{31}P} H^1_{^{31}P} = 2\pi\ 40\ \text{kHz}. \quad (1)$$

To improve the polarization transfer efficiency, the heteronuclear dipolar interaction averaged to zero by MAS was partly recoupled by a phase reversal applied in both channels at each half rotor period τ_r (Hediger et al. 1993). In these CP experiments, both ^{31}P and ^{1}H spectra were acquired. In the latter case, a spectrum without the CP irradiation at the ^{31}P frequency was also recorded as a reference, which made it possible to obtain, by difference, the signal from protons close to the phosphorus atoms.

RESULTS

X-ray powder diffraction

In the following text, starting-material stoichiometries will be referred to as x where x is the nominal Si-content (pfu) of the corresponding apatite formula. All syntheses yielded single-phase or near single-phase products with an apatite-like XRPD pattern (JCPDS 9-432). All observed diffraction peaks could be indexed in the $P6_3/m$ space group. $Ca(OH)_2$ and $CaSiO_3$ were detected as additional products for the silicate end-member composition (x = 6), and xenotime, YPO_4, for the x = 2 composition. The results of the cell-parameter refinement (Rietveld) are given in Table 1. The unit-cell volume was found to decrease almost linearly (by 1.5%) from the phosphate to the silicate apatite (Fig. 3). The change in unit-cell volume associated with the incorporation of yttrium and silicon is anisotropic and is mainly accommodated by the c-parameter ($\Delta c/c$ = –1.0%). The a-parameter is less sensitive ($\Delta a/a$ = –0.2%) to the substitution. The partitioning of Y between the Ca1 and Ca2 sites was tentatively addressed using Rietveld refinements. Atomic coordinates were taken either from the $P6_3/m$ cell of Kay et al. (1964) or from the $P2_1$ cell of Noe et al. (1993). In both cases, Y was found to partition preferentially into the Ca2 site. However, it should be noted that, whatever the composition, the yttrium partitioning between Ca1 and Ca2 strongly depends on the chosen asymmetric cell, with a much greater preference for the Ca2 site when hydroxylapatite atomic coordinates are used. Due to the slight differences between the two closely related atomic arrangements and also to the large number of atomic and site occupancy parameters (especially for the $P2_1$ cell), it appeared unrealistic to obtain reliable Y partition coefficients by using Rietveld refinement on our XRPD data. Furthermore, such a refinement was expected to be hampered by texture effects due to the needle-shape britholite habits as revealed by SEM imaging (Fig. 4). Therefore, Rietveld refinement was restricted here to the derivation of lattice constants.

TABLE 1. Hexagonal lattice constants along the OH-apatite–britholite-(Y) join

Nominal Si-content pfu (x)	a (Å)	c (Å)	V (Å^3)	Additional phases
0.0	9.419(2)	6.879(1)	528.5(3)	
0.5	9.413(2)	6.875(1)	527.5(3)	
1.0	9.412(3)	6.871(2)	527.1(5)	
2.0	9.407(4)	6.856(4)	525.4(7)	YPO_4
2.0	9.413(2)	6.863(1)	526.6(3)	
3.0	9.405(3)	6.848(3)	524.7(6)	
3.0	9.408(2)	6.840(1)	524.3(3)	
4.0	9.400(3)	6.831(3)	522.8(6)	
4.0	9.404(2)	6.837(1)	523.6(3)	
5.5	9.390(3)	6.810(3)	520.1(6)	
6.0	9.399(2)	6.808(1)	520.8(3)	$CaSiO_3$, $Ca(OH)_2$

Note: Samples with the same x are independent hydrothermal syntheses under identical P-T conditions. Cell-parameters are given to ±3σ where σ is the standard deviation given by DBW-9006PC.

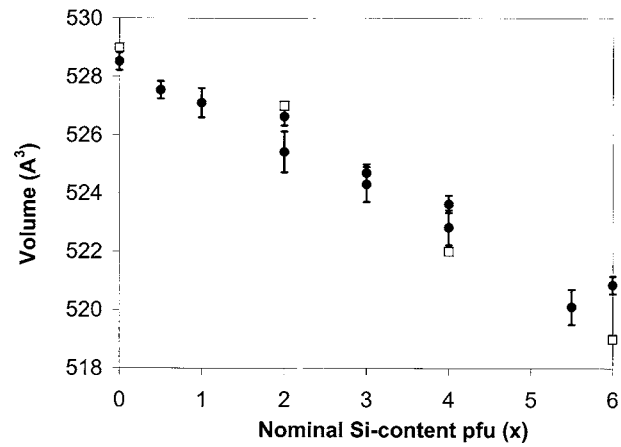

FIGURE 3. Unit-cell volume along the OH-apatite–britholite-(Y) series. Circles = this study; squares = Ito (1968).

FTIR spectroscopy

The hydroxylapatite infrared spectrum ($x = 0$) is characterized by a single absorption-band at 3572 cm^{-1} in the OH-stretching region (Fig. 5). The main effect of the Si and Y incorporation is a decrease of the 3572 cm^{-1} OH-stretching band intensity as well as the appearance of an unresolved band centered around 3545 cm^{-1} (Fig. 5). In the spectrum of the britholite end-member ($x = 6$), the 3572 cm^{-1} band is not observed. For that particular composition, an additional band occurs at 3644 cm^{-1} that is attributed to portlandite, $Ca(OH)_2$ (Busing and Morgan 1958). Furthermore, a marked decrease of the whole spectrum intensity is observed toward Si-rich compositions.

MAS NMR spectroscopy

^{1}H MAS NMR. ^{1}H MAS NMR spectra of synthetic members of the OH-apatite–britholite-(Y) series are displayed in Figure 6a. The ^{1}H spectrum of hydroxylapatite exhibits a line at 0.2 ppm as well as a sharp resonance at 5.0 ppm. When yttrium and silicon are incorporated into the structure two additional broad lines centered around 1.5 and 4.9 ppm are observed. For low silicon contents ($x = 0.5$, 2, and 3) the first line is centered at 1.5 ppm and shows a slight shoulder at around 1.2 ppm. With increasing silicon content ($x = 4$, 5, and 6), the line maximum is shifted to 2.0 ppm. The best fit of the broad 1.5 ppm resonance is obtained when it is decomposed into three lines at 1.2, 1.5, and 2.0 ppm (Fig. 7A). The respective intensity of these three lines depends on the amount of substitution.

^{31}P MAS NMR. The ^{31}P MAS NMR spectra of the various members of the series are displayed in Figure 6b. The ^{31}P spectrum of hydroxylapatite exhibits a single well-resolved resonance at 2.8 ppm. In silicon-bearing members, the 2.8 ppm line is still present but progressively broadens and displays a tail toward high fields. For phosphorus-dominant compositions, the broad 2.8 ppm line is simulated by two lines at 2.8 and 1.7 ppm. For silicon-dominant compositions, a broad component

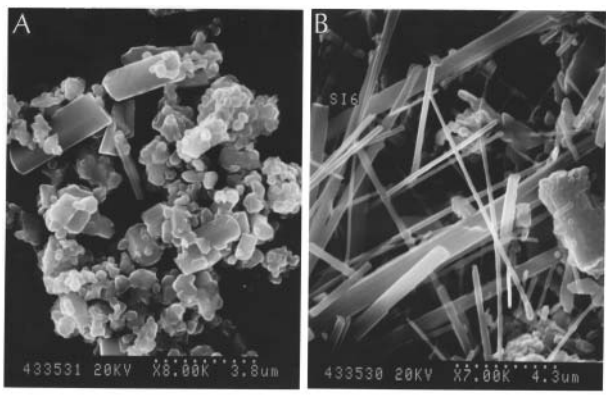

FIGURE 4. SEM images of two synthetic apatites (650 °C, 1.5 kbar, 15 days); (**b**) silicate end-member and (**a**) the intermediate composition with $x = 4$. Images are taken in secondary-electron mode using a Hitachi S-2500 microscope (ENS Paris).

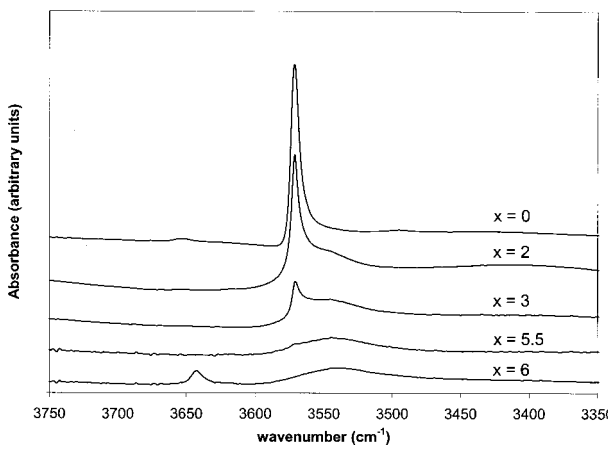

FIGURE 5. FT-IR spectra of members of the OH-apatite–britholite-(Y) series in the OH-stretching region. The same scale is used for all the samples, of identical weight.

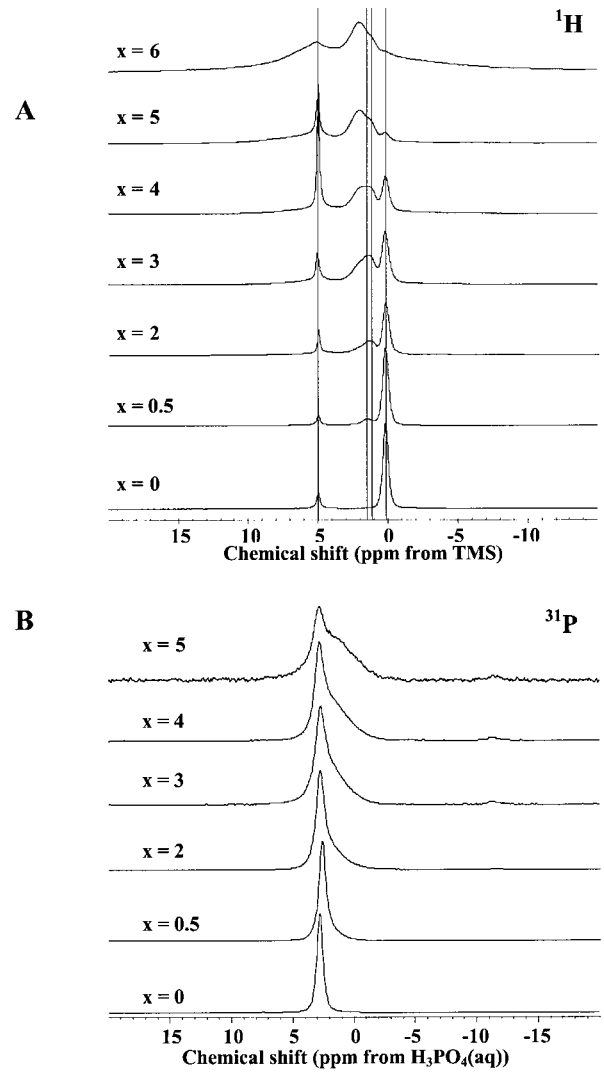

FIGURE 6. (**a**) ^{1}H and (**b**) ^{31}P MAS NMR spectra acquired at 300.13 MHz and 121.49 MHz, respectively, from the synthetic apatite samples after thermal treatment at 170 °C in air.

near 1.5 ppm is observed that requires simulation of two curves at 1.7 ppm and –0.6 ppm. The use of three different lines to fit the spectra (Fig. 7b) does not imply three well-defined phosphorus environments but rather indicates a distribution of isotropic chemical shifts induced by the substitution. An additional weak resonance is sometimes observed at –11.4 ppm, which is likely to represent an extra phase.

^{1}H-^{31}P cross polarization. The one dimensional (1D) ^{31}P MAS and ^{1}H-^{31}P CP/MAS NMR spectra are similar except that the –11.4 ppm resonance is absent from the latter. The difference between ^{1}H MAS spectra obtained without and with ^{1}H-^{31}P CP contact indicates that the protons characterized by the ^{1}H line at 0.2 ppm and those centered around 1.5 ppm transfer magnetization to ^{31}P. However, there is no polarization transfer from the very strong ^{1}H line at 5.0 ppm to any ^{31}P line.

^{1}H MAS NMR of heated samples. Some of the synthetic samples were heated in air and characterized using ^{1}H MAS NMR. Whatever the sample composition (x = 0, 4, or 6), a significant weight loss, around 1 wt%, is encountered between 500 and 550 °C. On ^{1}H NMR spectra of the corresponding samples, this event is characterized by the disappearance of the 5.0 ppm line. The shape and the absolute intensities of the other ^{1}H lines remain unchanged.

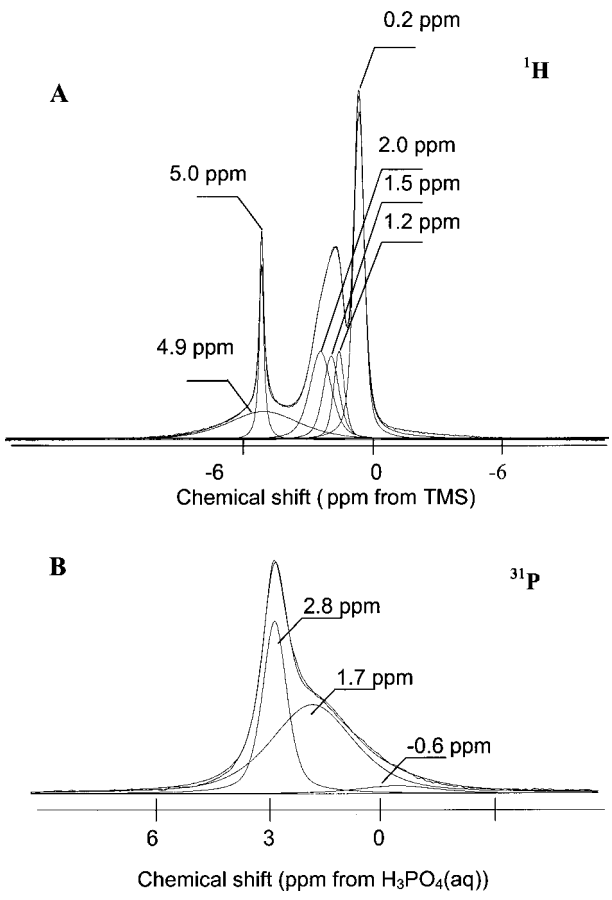

FIGURE 7. Simulation details of an (**a**) ^{1}H MAS NMR and (**b**) a ^{31}P MAS NMR spectrum.

DISCUSSION

Lattice parameters variation

Unit-cell volume data compare well with those obtained by Ito (1968) for apatites with identical nominal compositions (Fig. 3). The relative volume variation of –1.5% encountered along the series appears rather weak when compared to the +8.4% value obtained by Boyer et al. (1997) for the synthetic fluorapatite–britholite-(La) series (in an OH-free system). This difference can be related to the size of the trivalent cation, Y^{3+} vs. La^{3+}, involved in the coupled substitution. The net ionic-radius change of the $LaSiCa_{-1}P_{-1}$ substitution is 0.13 Å whereas that of the $YSiCa_{-1}P_{-1}$ substitution is –0.02 Å (ionic radii are taken from Shannon 1976)

Additional phases revealed by the spectroscopic data

Spectroscopic measurements (NMR and IR) allowed detection of extra phases in products that were identified as single phase by X-ray powder diffraction.

Fluid inclusions. In hydroxylapatite synthesized by precipitation, Yesinowski and Eckert (1987) observed a sharp ^{1}H NMR line at 5.6 ppm with no sideband. They assigned it to protons from adsorbed water molecules. In our synthetic samples, a resonance with similar characteristics was found at 5.0 ppm. The corresponding protons are therefore mobile. In addition, this resonance shows no polarization transfer to any ^{31}P in the CPMAS experiments. However, temperatures as high as 500–550 °C (in air) are required to make this resonance disappear. This resonance cannot therefore be attributed to protons from adsorbed water molecules. Concomitantly to the disappearance of this line, a weight loss is observed (likely to be a water loss), which does not alter the apatite structure. The ^{1}H NMR line at 5.0 ppm therefore represents protons from water molecules that are not bonded to the apatite structure. These water molecules likely belong to water inclusions.

Xenotime and portlandite. A weak ^{31}P resonance was observed at –11.4 ppm for intermediate compositions (x = 2, 3, and 4). This resonance is attributed to YPO_4, xenotime, by comparison with independent ^{31}P MAS NMR measurements performed on synthetic xenotime. This is corroborated by (1) the identification of xenotime in one of these products (x = 2) using X-ray powder diffraction, and (2) the CPMAS data that show no polarization transfer between any apatite protons and this –11.4 ppm ^{31}P line.

The 3644 cm^{-1} band observed in the infrared spectrum of the britholite-(Y) end-member is attributed to $Ca(OH)_2$, portlandite (Busing and Morgan 1958).

Proton environment from FTIR spectroscopy

The 3572 cm^{-1} OH-stretching band is commonly found in hydroxylapatite IR spectra. To our knowledge, the only available IR data for a pure OH-britholite were published by Ito (1968). He obtained a single OH-stretching band at 3540 cm^{-1} for a synthetic $Ca_4Dy_6(SiO_4)_6(OH)_2$ britholite. In our synthetic end-member britholite-(Y), a similar band was found but it is located at approximately 3545 cm^{-1} (Fig. 5). This slight wavenumber difference seems to indicate that OH-stretching vibration frequency is sensitive to the trivalent cation.

OH-stretching wavenumbers around 3545 cm^{-1} reflect very weak hydrogen bonding, if any (Libowitzky 1999). Therefore OH-stretching vibration will be mostly controlled by the neighboring cationic environment (Beckenkamp and Lutz 1992; Libowitzky 1999). Actually, the greater width of the 3545 cm^{-1} band probably reflects various cationic environments, i.e., one, two, or three Y atoms in the close neighborhood of the hydroxyl group.

With respect to the decrease in observed bulk intensity, if a constant absorption coefficient is assumed for the OH vibration along the series in the 3500–3600 cm^{-1} range, then the occurrence of proton vacancies must be considered. Consequently, new OH environments as ···OH-O-HO··· and/or ···OH-O-OH··· must arise, the corresponding OH-stretching bands of which should also contribute to the broad 3545 cm^{-1} band.

Proton vacancies along the synthetic apatite-britholite series

Variations in the bulk hydrogen content between various samples can be estimated from ^{1}H NMR spectra using the sum of the intensity of the apatite ^{1}H lines (i.e., 0.2, 1.2, 1.5, 2.0, and 4.9 ppm). This procedure clearly yields a total intensity that decreases from the phosphate to the silicate end-member (Fig. 8). Therefore, as already suggested by the IR data, the proton content must decrease along the synthetic series. The total proton loss from the phosphate to the silicate end-member is estimated to be around 50%.

Partial occupancy of the proton site will therefore have to be taken into account when interpreting the ^{1}H NMR spectra. Trombe (1973) has proposed that, upon heating, hydroxylapatite transforms into an oxyapatite, $Ca_{10}(PO_4)_6(OH)_{2-2x}O_x$, which re-hydrates in air upon cooling. Moreover, with respect to silicate apatites, Ito (1968) synthesized a large number of oxyapatites, $(Me^{2+}_{1-y}, Me^{3+}_{y})_{10}[(P_{1-x},Si_x)O_4]_6O_2$ with $y = (3x + 1)/5$. These included Y-bearing apatites of $Ca_2Y_8Si_6O_{26}$, $Ca_4Y_6Si_4P_2O_{26}$, $Ca_6Y_4Si_2P_4O_{26}$, and $Ca_8Y_2P_6O_{26}$ compositions, synthesized at 1200 °C in air.

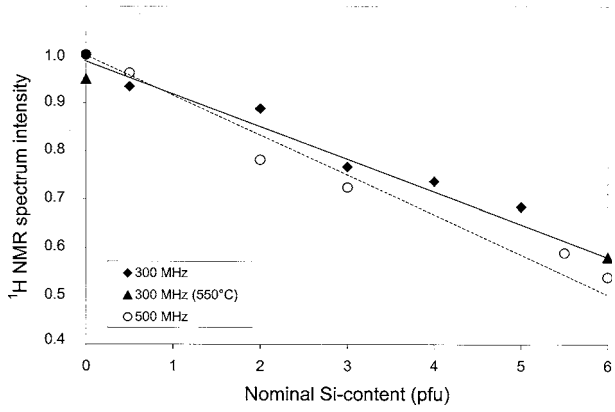

FIGURE 8. Bulk intensity of the ^{1}H MAS NMR spectra normalized to hydroxylapatite as a function of the nominal Si-content pfu. Only the 5.0 ppm band is ignored because it corresponds to protons that are not bonded to the apatite structure. The solid line is the least squares regression of the data. For calculation purposes (see text), proton content (pfu) is approximated to $2 - x/6$ (dashed line).

According to these results, $Ca^{2+} + H^+ = Y^{3+} + \square$ is a possible substitution component in the apatite structure. This substitution is likely to occur in our synthetic compounds and could account for the low hydrogen content of the Y-rich compositions. As a consequence, the composition of our synthetic apatites must deviate from that of the starting material (nominal composition). This assumption is corroborated by the presence of $CaSiO_3$ as an additional phase detected in the XRPD pattern of Y-rich compositions.

To take this substitution component into account, we introduce a second variable parameter y and the apatite formula is then written:

$$Ca_{10-(x+y)}Y_{x+y}(PO_4)_{6-x}(SiO_4)_xO_2H_{2-y} \quad (2)$$

where x corresponds to the number of yttrium atoms pfu (per formula unit) incorporated according to the $YSiCa_{-1}P_{-1}$ substitution. The y coefficient represents yttrium atoms substituted for Ca and charge-balanced by proton vacancies, i.e., the extent of the $Ca^{2+} + H^+ = Y^{3+}$ substitution. On the basis of the total ^{1}H NMR intensity (Fig. 8), the proton content was found to decrease linearly from the phosphate to the silicate end-member by around 50%, i.e., $y \sim x/6$. This leads to the approximate formula $Ca_{10-7x/6}Y_{7x/6}(PO_4)_{6-x}(SiO_4)_xO_2H_{2-x/6}$.

Interpretation of the ^{31}P NMR spectra

The ^{31}P NMR spectrum of hydroxylapatite shows a single well-resolved resonance at 2.8 ppm. An additional broad signal centered around 1.5 ppm occurs along the series that is modeled as the sum of two lines at 1.7 and –0.6 ppm. However, this signal is interpreted as originating from a distribution of various phosphorus atom environments rather than from a contribution of two distinct environments.

The PO_4 tetrahedra are made of two O3 atoms, one O1 atom, and one O2 atom. Each phosphorus atom shares four O atoms with nine calcium polyhedra, five of which are Ca2 positions. Because the 2.8 ppm resonance is the only resonance observed in hydroxylapatite, in agreement with previous studies (e.g., Rothwell et al. 1980), it is tempting to assign it to phosphorus atoms with nine Ca as close neighbors. In that case, the 1.7 and –0.6 ppm lines would reflect phosphorus atoms with one of the nine Ca atoms, at a minimum, replaced by a Y atom.

Assuming a random distribution of Y atoms over the Ca1 and Ca2 sites, the relative intensity of the 2.8 ppm ^{31}P NMR line for a given apatite composition [i.e., the probability, P(9Ca,x,y), of having a nine-Ca environment for a given composition] is:

$$P(9Ca,x,y) = \left(\frac{10-(x+y)}{10}\right)^9 \quad (3)$$

where x and y are the parameters defined in formula 2.

According to this calculation and assuming that $y = x/6$, the intensity of the 2.8 ppm line must decrease very rapidly to reach values lower than 1% intensity for Si contents (x) higher than 3.5 atoms pfu. This trend does not fit the experimental data because the 2.8 resonance still contributes

to around 15% of the total band intensity in the silicate end-member spectrum (Fig. 9).

This calculation assumes a random distribution of Y and Ca atoms over the Ca1 and Ca2 sites, although preferential partitioning may occur. The preliminary Rietveld refinement results obtained here as well as the study of Khudolozhkin et al. (1973) on the synthetic apatite–britholite-(Y) series (with only F in the halogen site), have shown that if partitioned, Y atoms would preferentially enter the Ca2 site. Consequently, if partitioning occurs, it will lower the calculated intensity of the 2.8 ppm line because, around a given phosphorus atom, the proportion of Ca2 sited (5/9) is greater than that of Ca1 (4/9).

Therefore the primary assumption that the 2.8 ppm line represents phosphorus atoms surrounded by Ca atoms alone is inappropriate and cannot account for the experimental data. The latter intensity calculation shows that this line must also reflect additional, Y-bearing phosphorus environments. In other words, some phosphorus atoms involved in P-O-Y bonds must also contribute to the 2.8 ppm line intensity.

The major structural difference between hydroxylapatite and britholite-(Y) that may directly influence the phosphorus environment resides in the position of the O3 atoms (Noe et al. 1993). The shift of the O3 atoms is interpreted by Noe et al. (1993) as a way of increasing bonding to the Ca1 and Ca2 sites. In ternary OH, F, Cl-apatites, only the P-O3 bond distances and P-O3-P angles show a systematic variation correlative with the Cl-content (Hughes et al. 1991). The 1.7 ppm and –0.6 ppm bands could therefore be related to changes in O3 bonding in response to REE-Ca replacement or, eventually, to the occurrence of proton vacancies. Each tetrahedron possesses two O3 atoms that are bonded to three Ca2 atoms, one at 2.94 Å and two at 3.71 Å, and two Ca1 atoms at 3.20 Å (Noe et al. 1993). Thus, considering those five calcium atoms the probability (Fig. 9) to have a 5Ca environment (i.e., the relative intensity of the 2.8 ppm line) is:

$$P(5Ca,x,y) = \left(\frac{10-(x+y)}{10}\right)^5 \quad (4)$$

Again the calculated intensity is too low compared to the ^{31}P NMR experimental data. The agreement becomes excellent when we assume that only two (rather than five) of the nine Ca sites must be filled with Ca to contribute to the 2.8 ppm line. However, we do not see any crystal-chemical justification for this result, which could merely be fortuitous. Structural refinement of apatites with intermediate compositions is required to further interpret the ^{31}P NMR data.

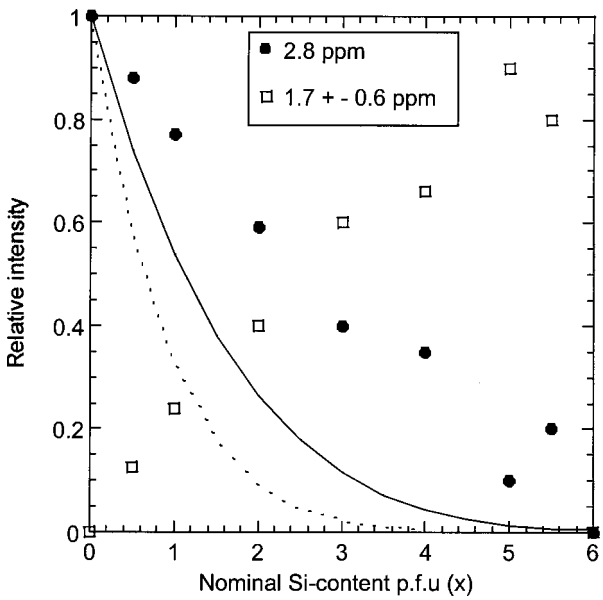

FIGURE 9. Relative intensity of the ^{31}P MAS NMR resonances plotted against nominal Si-content pfu. The dotted and solid lines represent P(9Ca,*x*,*y*) and P(5Ca,*x*,*y*) probability functions, respectively (see text). No yttrium partitioning is considered between the two Ca sites.

Interpretation of the ^{1}H NMR spectra

As previously observed by Yesinowski and Eckert (1987), protons in hydroxylapatite are characterized by a single ^{1}H NMR resonance at 0.2 ppm. Whereas a single proton-site is inferred in hydroxylapatite from ^{1}H NMR data, up to five proton environments are found in Si-bearing compositions. Therefore ^{1}H NMR is more sensitive than ^{31}P to the crystal-chemical changes that occur along the series. Because of the expected absence of significant hydrogen bonding in apatite (see above), the chemical shift of the hydroxyl protons will be mostly sensitive to the cationic environment of the donor O atom (O_H). This donor O atom is bonded to three cations from the Ca2 site, Ca and/or Y atoms. Consequently, there are four possible close environments for a given O_H (and H) atom, designated [3Ca], [2CaY], [Ca2Y], and [3Y]. Apart from the resonance at 0.2 ppm, which is unambiguously attributed to [3Ca] environments, assignment of the other ^{1}H NMR lines to these different proton environments is not straightforward. Furthermore, the presence of five distinct lines may indicate additional ^{1}H environments. ^{1}H NMR might be sensitive to the distribution of second-shell atoms (i.e., phosphorus and silicon) and possibly to the effect of adjacent proton vacancies. The abundance of a given environment is directly related to the intensity of the corresponding resonance(s). The probability that a given environment occurs in the apatite channel is a function of apatite composition and can be calculated using a binomial law assuming that site occupancy (Ca or Y) is a discrete random variable (see Appendix 1). The comparison between measured line intensity and calculated environment abundance along the series brings valuable constraints to any assignment model. By "resonance intensity" we mean the following: absolute resonance intensity normalized to the bulk intensity of a hydroxylapatite spectrum acquired under identical experimental conditions. The bulk intensity of a normalized spectrum is then proportional to the bulk proton content of the sample, the good simulation of which is another important constraint to the line assignment. Based on the trend of resonance intensity variation along the series (Fig. 10), three groups of bands can be distinguished. From the phosphate to the silicate end-member, the 0.2 ppm resonance shows a strongly decreasing intensity. The intensity of the 1.2

and 1.5 ppm resonances increases for P-dominant compositions and then decreases down to almost zero at the silicate end-member composition. The intensity of the 2.0 and 4.9 ppm resonances increases regularly toward the silicate end-member. If one tries to match these measured trends to the calculated [(*n*)Ca(3–*n*)Y] environment abundance (see Appendix 1), the 1.2 ppm and 1.5 ppm lines are attributed to [2CaY] environments and the 2.0 and 4.9 ppm lines to Y-rich ones, possibly [Ca2Y] and [3Y], respectively, assuming a chemical shift that would decrease with *n* (Fig. 10).

This preliminary assignment gives rise to two main problems. (1) The [2CaY] environment generates two resonances whereas the other environments contribute to a single line. (2) The [3Ca], [2CaY], and [Ca2Y] arrangements are characterized by sharp lines found at nearly equally spaced chemical shifts whereas the 4.9 ppm line [3Y] is extremely broad and found at much lower field. Furthermore, although trends are well matched, measured and calculated intensities do not coincide. We have therefore tested additional assignments. Protons were either evenly distributed in the channel or preferentially attached to specific [(*n*)Ca(3–*n*)Y]O groups. The effect of Y partitioning between the Ca1 and Ca2 sites was also considered. We will describe here our preferred assignment model based on agreement between calculated and observed intensities and crystal-chemical significance. However, due to experimental uncertainties and the variety of possible atomic arrangements within the channel, this model cannot be considered as unique.

The intensity and the specificity of the 4.9 ppm resonance (broadness and low field position) suggest that this line does not only reflect the influence of the O_H cationic environment ([(*n*)Ca(3–*n*)Y]), as is the case for the other resonances. Both line position and width could suggest molecular water trapped in the apatite columns. However, the absence of significant spinning sidebands rules out this possibility (Yesinowski et al. 1988). Actually, the intensity of the 4.9 ppm line increases regularly toward the silicate end-member as does the number of H vacancies. In isotropic chemical shift-hydrogen bonding correlation (e.g., Yesinowski and Eckert 1987), a chemical shift of 4.9 ppm is close to the limit from which hydrogen bonding, although very weak, can be considered. Thus, we propose that the unprotonated O_H anions in the channel can act as acceptor O atoms for hydrogen bonding (as previously proposed by Taitai and Lacout 1987).

To properly simulate the 0.2 ppm line intensity, one must assume that all O_H atoms from [3Ca] environments are protonated. In other words, proton vacancies cannot be evenly distributed over all the [(*n*)Ca(3–*n*)Y] environments. This is a quite plausible assumption because, to our knowledge, hydrogen deficiency has never been reported in hydroxylapatite synthesized hydrothermally at temperatures as low as 650 °C. Conversely, when Y^{3+} substitutes for Ca^{2+} in the Ca2 site, hydrogen vacancies can be seen as an alternative mechanism to achieve local charge-balance.

The exact distribution of the H vacancies over the three remaining environments (i.e., [2CaY], [Ca2Y] and [3Y]) cannot be resolved by our data and therefore the vacancies were evenly distributed. The resulting assignment is summarized in Table 2 and leads to an excellent agreement between experimental and calculated intensities (Fig. 10). The abundance calculations used to derive these intensities are presented in Appendix 1. For that assignment, we assumed that the protons that give rise to the 4.9 ppm resonance can belong to [3Ca], [2CaY], [Ca2Y], or [3Y] environments. This is consistent with the large resonance-width, which is comparable to the spread of chemical shifts between the 0.2 and the 2.0 ppm lines. In the same manner, the 2.0 ppm line, which is relatively broad, is attributed in this latter model to two different proton-environments ([Ca2Y] and [3Y]). The diversity of next-neighbor configurations in Y-rich environments could be the reason for the poor resolution. For [2CaY], ^{1}H NMR spectroscopy seems to be able to partly resolve these second-shell environments as shown by the occurrence of two resonances (1.2 and 1.5 ppm, Table 2).

TABLE 2. ^{1}H NMR resonances, assignment and characteristics

^{1}H NMR isotropic resonance (ppm)	Line-width (Hz)	Assignment
0.2	150	[3Ca]*
1.2	189	[2CaY]*
1.5	282	[2CaY]*
2.0	384	[Ca2Y]* and [3Y]*
4.9	1290	[3Ca]†, [2CaY]†, [Ca2Y]†, and [3Y]†
5.0	70	water inclusions

* Protons pointing towards a protonated O_H atom.
† Protons pointing towards an unprotonated O_H atom.

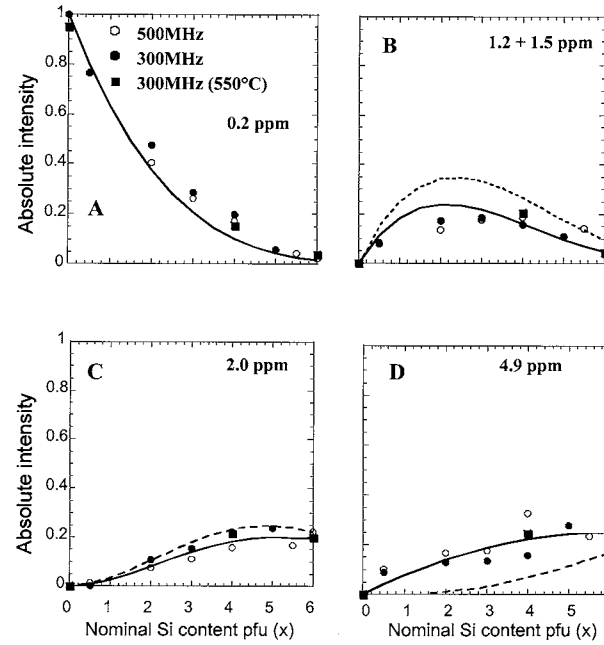

FIGURE 10. Absolute intensity of each ^{1}H NMR resonance (normalized to hydroxylapatite) vs. nominal Si-content pfu with a number of vacancy (pfu) set to *x*/6. Dashed lines represent the calculated intensities (see Appendix 1) for the first assignment, i.e., 0.2 ppm to [3Ca], 1.2 + 1.5 ppm to [2CaY], 2.0 ppm to [Ca2Y], and 4.9 ppm to [3Y], with proton vacancies randomly distributed over all [*n*Ca(3–*n*)Y] environments. Solid lines represent the preferred assignment model (see text) with proton vacancies randomly distributed over the [2CaY], [Ca2Y], and [3Y] environments.

It should be noted that it has been assumed that the probability for a given proton to face a particular configuration (protonated and unprotonated) is proportional to the abundance of that particular configuration (see Appendix 1). In other words, possible interactions between the different configurations that would lead to the occurrence of peculiar configuration sequences (e.g., [3Ca] clusters) along the **c** axis have been ignored.

Implications for natural britholites

The main result of this study is the identification of proton deficiency in Si-bearing apatites synthesized at 650 °C, 1.5 kbar under hydrothermal conditions. The oxyapatite substitution-component believed to only proceed at high temperatures (above 800 °C in air) can potentially occur in natural silicate apatites as well. Admittedly, natural britholites are fluorine-rich and this substitution would only apply to the OH component. Nonetheless, this study should prompt the re-investigation of the chemistry of natural britholite as well as additional syntheses and characterization in F-bearing silicate-apatite systems. Interestingly, electron-microprobe analyses reported by Orlandi et al. (1989) for britholite-(Ce) crystals from Mt Vesuvius are consistent with "oxybritholite" compositions. The ^{1}H NMR assignment model developed in this study can serve as a basis for further experimental investigations and especially for interpreting the complex apatite dehydration process. Unfortunately, the paramagnetic nature of REE, major constituents of natural silicate-apatites, may limit the NMR investigation of other britholite compositions.

Acknowledgments

We gratefully acknowledge B.L. Sherriff and an anonymous reviewer for their constructive reviews that greatly improved the manuscript. L. Mamou is warmly thanked for running the X-ray powder diffractometer at ENS. Financial support was provided by the CEA/CNRS NOMADE research program.

References cited

Baddiel, C.B. and Berry, E.E. (1966) Spectra structure correlations in hydroxy and fluoroapatites. Spectrochimica Acta, 22, 1407–1416.

Baumer, A., Guilhot, B., Gibert, R., Vernay, A.M., and Ohnenstetter, D. (1994) Détection des ions chlore et fluor dans les apatites par spectrométrie infrarouge. Comptes Rendus de l'Acadamie des Sciences Paris, 319, série II, 193–200.

Beckenkamp, K. and Lutz, H.D. (1992) Lattice vibration spectra. Part LXXII. OH stretching frequencies of solid hydroxides – correlation with structural and bonding data. Journal of Molecular Structure, 270, 393–405.

Belton, P.S., Harris, R.K., and Wilkes, P.J. (1988) Solid state phosphorus-31 NMR studies of synthetic inorganic calcium phosphates. Journal of Physics and Chemistry of Solids, 1, 21–27.

Boyer, L., Carpena, J., and Lacout, J.L. (1997) Synthesis of phosphate-silicate apatites at atmospheric pressure. Solid State Ionics, 95, 121–129.

Brunet, F., Allan, D.R., Redfern, S.A.T., Angel, R.J., Miletich, R., Reichmann, H.J., Sergent, J., and Hanfland, M. (1999) Compressibility and thermal expansivity of synthetic apatites, $Ca_5(PO_4)_3X_2$ with X = OH, F, and Cl. European Journal of Mineralogy, 11, 1023–1035.

Busing, W.R. and Morgan, H.W. (1958) Infrared spectrum of $Ca(OH)_2$. Journal of Chemical Physics, 28, 998–999.

Chopin, C. and Sobolev, N.V. (1995) Principal mineralogical indicators of UHP in crustal rocks. In R.G. Coleman and X. Wang, Eds., Ultrahigh-pressure metamorphism, p. 96–131. Cambridge University Press, Cambridge, U.K.

Della Ventura, G., Williams, C.T., Cabella, R., Oberti, R., Caprilli, E., and Bellatreccia, F. (1999) Britholite-hellandite intergrowths and associated REE-minerals from the alkali-syenitic ejecta of the Vico volcanic complex (Latium, Italy): petrological implications bearing on REE mobility in volcanic systems. European Journal of Mineralogy, 11, 843–854.

Elliott, J.C. (1964) The crystallographic structure of dental enamel and related apatites. Ph.D. dissertation, University of London.

Elliott, J.C., Mackie, P.E., and Young, R.A. (1973) Monoclinic hydroxyapatite. Science, 180, 1055–1057.

Engel, G. and Klee, W.E. (1972) Infrared spectra of the hydroxyl ions in various apatites. Journal of Solid State Chemistry, 5, 28–34.

Fleischer, M. and Altschuler, Z.S. (1986) The lanthanides and yttrium in minerals of the apatite group. An analysis of the available data. Neues Jahrbuch für Mineralogie Monatshefte, 10, 467–480.

Freund, F. and Knobel, R.M. (1976) Distribution of fluorine in hydroxyapatite studied by infrared spectroscopy. Journal of the Chemical Society, Dalton Transactions, 1136–1140.

Gonzales-Diaz, P.F. and Santos, M. (1977) On the hydroxyl ions in apatites. Journal of Solid State Chemistry, 22, 193–199.

Hartmann, S.R. and Hahn, E.L. (1962) Nuclear double resonance in the rotating frame. Physical Reviews, 128, 2042–2053.

Hediger, S., Meier, B.H., and Ernst, R.R. (1993) Cross polarization under fast magic angle spinning using amplitude-modulated spin lock sequences. Chemical Physics Letters, 213, 627–635.

Hughes, J.M., Cameron, M., and Crowley, K.D. (1989) Structural variations in natural F, OH, and Cl apatites. American Mineralogist, 74, 870–876.

Hughes, J.M., Cameron, M., and Mariano, A.N. (1991) Rare-earth element ordering and structural variations in natural rare-earth-bearing apatites. American Mineralogist, 76, 1165–1173.

Ito, J. (1968) Silicate apatites and oxyapatites. American Mineralogist, 53, 890–907.

Jamtveit, B., Dahlgren, S., and Austrheim, H. (1997) High-grade contact of metamorphism of calcareous rocks from the Oslo rift, southern Norway. American Mineralogist, 82, 1241–1254.

Kalsbeek, N., Larsen, S., and Rønsbo, J.G. (1990) Crystal structures of rare earth element-rich apatite analogues. Zeitschrift für Kristallographie, 191, 249–263.

Kay, M.I., Young, R.A., and Posner, A.S. (1964) Crystal structure of hydroxylapatite. Nature, 204, 1050–1052.

Khudolozhkin, V.O., Urusov, V.S., and Tobelko, K.I. (1973) Dependence of structural ordering of rare earth atoms in the isomorphous series apatite-britholite (abukumalite) on composition and temperature. Geochemistry International, 10, 1171–1177.

Libowitzky, E. (1999) Correlation of O-H···O hydrogen bond lengths in minerals. Monatshefte für Chemie, 130, 1047–1059.

Mariano, A.N. (1989) Economic geology of rare earth minerals, In B.R. Lipin and G.A. McKay, Eds., Rare Earth Elements, vol. 21. Reviews in mineralogy, Mineralogical Society of America, Washington D.C.

Massiot, D., Thiele, H., and Germanus, A. (1994) WinFit—a Windows-based program for lineshape analysis. Bruker Report, 140, 43–46.

Matchatshki, F. (1939) Sind Abukumalit und Britholit glieder der Apatit-reihe? Zentralblatt für Mineralogie, A, 161–164.

McConnell, D. (1973) Apatite. Its crystal chemistry, mineralogy, utilization and biologic occurrence, Springer Verlag, New York.

Moore, P.B. (1984) Crystal-chemical aspects of the phosphate minerals. In J.O. Nriagu and P.B. Moore, Eds., Phosphate minerals, p. 155–170, Springer Verlag, Berlin.

Murayama, J.K., Nakai, S., Kato, M., and Kumazawa, M. (1986) A dense polymorph of $Ca_3(PO_4)_2$: A high pressure phase of apatite decomposition and its geochemical significance. Physics of the Earth and Planetary Interiors, 44, 293–303.

Noe, D.C., Hughes, J.M., Mariano, A.N., Drexler, J.W., and Kato, A. (1993) The crystal structure of monoclinic britholite-(Ce) and britholite-(Y). Zeitschrift für Kristallographie, 206, 233–246.

Orlandi, P., Perchiazzi, N., and Mannucci, G. (1989) First occurrence of britholite-(Ce) in Italy (Monte Somma, Vesuvius). European Journal of Mineralogy, 1, 723–725.

Ouzegane, K., Fourcade, S., Kienast, J.R., and Javoy, M. (1988) New carbonatite complexes in the Archaean In'Ouzzal nucleus (Ahaggar, Algeria): mineralogical and geochemical data. Contributions to Mineralogy and Petrology, 98, 277–292.

Rothwell, W.P., Waugh, J.S., and Yesinowski, J.S. (1980) High resolution variable temperature ^{31}P NMR of solid calcium phosphates. Journal of the American Chemical Society, 102, 2637–2643.

Sakthivel, A. and Young, R.A. (1991) Programs DBWS-9006 and DBWS-9006PC for Rietveld analysis of X-Ray and neutron diffraction patterns.

Shannon, R.D. (1976) Revised effective ionic radii and systematic studies of interatomic distances in halides and chalcogenides. Acta Crystallographica A, 32, 751–767.

Sudarsanan, K., Mackie, P.E., and Young, R.A. (1972) Comparison of synthetic and mineral fluoroapatite, $Ca_5(PO_4)_3F$, in crystallographic detail. Materials Research Bulletin, 7, 1331–1338.

Taitai, A. and Lacout, J.L. (1987) Hydroxylation and fluorination of europium containing oxyapatites. Journal of Physics and Chemistry of Solids, 48, 629–633.

Trombe, J.C. (1973) Contribution à l'étude de la décomposition et de la réactivité de certaines apatites hydroxylées et carbonatées. Annales de Chimie, 8, 251–269.

Yesinowski, J.P. and Eckert, H. (1987) Hydrogen environments in calcium phosphates: ^{1}H MAS NMR at high spinning speeds. Journal of the American Chemical Society, 109, 6274–6282.

Yesinowski, J.P., Eckert, H., and Rossman, G.R. (1988) Characterization of hydrous species in minerals by high speed ^{1}H MAS-NMR. Journal of the American Chemical Society, 110, 1367–1375.

MANUSCRIPT RECEIVED MAY 7, 2001
MANUSCRIPT ACCEPTED JANUARY 28, 2002
MANUSCRIPT HANDLED BY JOHN RAKOVAN

APPENDIX 1: SIMULATION OF ^{1}H RESONANCE INTENSITY

The series formula used in the following is

$$Ca_{10-(x+y)}Y_{x+y}(PO_4)_{6-x}(SiO_4)_xO_2H_{2-y}$$

Making the assumption of a random distribution of Y and Ca atoms over the six Ca2 and four Ca1 sites, the probability P(nCa,x,y) that an O_H atom is bonded to a [(n)Ca(3–n)Y] configuration [i.e., to be bonded to (n) calcium and (3–n) yttrium atoms] is:

$$P(n\mathrm{Ca},x,y) = C_3^n\left\{\left(\frac{10-(x+y)}{10}\right)^n\left(\frac{x+y}{10}\right)^{3-n}\right\}$$

If we assume that [3Ca] environments have no vacancy in their vicinity and that hydrogen vacancies are randomly distributed over the three other [(n)Ca(3–n)Y] environments, the probability to find a proton vacancy on a given [(n)Ca(3–n)Y] environment with $n < 3$ is

$$P(\square,n\mathrm{Ca},x,y) = \frac{y}{2}\left(\frac{1}{P(2\mathrm{Ca},x,y)+P(1\mathrm{Ca},x,y)+P(0\mathrm{Ca},x,y)}\right)$$

Then, $I_{0.2\ ppm} = I(3\mathrm{Ca},x,y) = P(3\mathrm{Ca},x,y)[1 - P(\square,3\mathrm{Ca},x,y)](2 - y)/2$ where $I(3\mathrm{Ca},x,y)$ is the 0.2 ppm line intensity normalized to the bulk intensity of a hydroxylapatite spectrum. In the particular case of the 0.2 ppm resonance attributed to [3Ca] environments, $P(\square,3\mathrm{Ca},x,y) = 0$ because none of the [3Ca] O atoms are unprotonated (see text).

In the same manner, the calculated intensity of the 1.2 and 1.5 resonance sum is :

$I_{1.2 + 1.5\ ppm} = I(2\mathrm{Ca},x,y) = P(2\mathrm{Ca},x,y)[1 - P(\square,2\mathrm{Ca},x,y)](2 - y)/2$

and $I_{2.0\ ppm} = I(1\mathrm{Ca},x,y) + I(0\mathrm{Ca},x,y)$

with $I(1\mathrm{Ca},x,y) = P(1\mathrm{Ca},x,y)[1 - P(\square,1\mathrm{Ca},x,y)](2 - y)/2$

and $I(0\mathrm{Ca},x,y) = P(0\mathrm{Ca},x,y)[1 - P(\square,0\mathrm{Ca},x,y)](2 - y)/2$

Calculation of the 4.9 ppm line intensity is different because it results from the contribution of all [(n)Ca(3–n)Y] environments with $n < 3$ that face an unpronated O_H atom:

$$I_{4.9\ ppm} = \sum_{n=0}^{n=3} P(n\mathrm{Ca},x,y)[1 - P(\square,n\mathrm{Ca},x,y)]\frac{y}{2} = \left(1-\frac{y}{2}\right)\frac{y}{2}\ .$$